Received: 16 November 2018 | Revised: 18 January 2019 | Accepted: 8 February 2019

DOI: 10.1002/btpr.2785

RESEARCH ARTICLE

BIOTECHNOLOGY PROGRESS

Using CFD simulations and statistical analysis to correlate oxygen mass transfer coefficient to both geometrical parameters and operating conditions in a stirred-tank bioreactor

Momen Amer | Yu Feng | Joshua D. Ramsey

Chemical Engineering, Oklahoma State University, Stillwater, Oklahoma

Correspondence
Joshua D. Ramsey, Chemical Engineering, Oklahoma State University, Stillwater, Oklahoma 74078.
Email: josh.ramsey@okstate.edu

Optimization of a bioreactor design can be an especially challenging process. For instance, testing different bioreactor vessel geometries and different impeller and sparger types, locations, and dimensions can lead to an exceedingly large number of configurations and necessary experiments. Computational fluid dynamics (CFD), therefore, has been widely used to model multiphase flow in stirred-tank bioreactors to minimize the number of optimization experiments. In this study, a multiphase CFD model with population balance equations are used to model gas–liquid mixing, as well as gas bubble distribution, in a 50 L single-use bioreactor vessel. The vessel is the larger chamber in an early prototype of a multichamber bioreactor for mammalian cell culture. The model results are validated with oxygen mass transfer coefficient (k_La) measurements within the prototype. The validated model is projected to predict the effect of using ring or pipe spargers of different sizes and the effect of varying the impeller diameter on k_La. The simulations show that ring spargers result in a superior k_La compared to pipe spargers, with an optimum sparger-to-impeller diameter ratio of 0.8. In addition, larger impellers are shown to improve k_La. A correlation of k_La is presented as a function of both the reactor geometry (i.e., sparger-to-impeller diameter ratio and impeller-to-vessel diameter ratio) and operating conditions (i.e., Reynolds number and gas flow rate). The resulting correlation can be used to predict k_La in a bioreactor and to optimize its design, geometry, and operating conditions.

KEYWORDS
computational fluid dynamics, stirred-tank bioreactor, mass transfer coefficient, mixing, population balance model

1 | INTRODUCTION

The first single-use bioreactor was introduced in the late 1990s as a plastic bag that is mixed via wave motion.[1] Since then, single-use bioreactors have gathered a great deal of interest and been hugely successful in replacing their stainless steel counterparts for upstream processing in the biopharmaceutical industry.[2] While wave-mixed bioreactors initially dominated the single-use technology market, stirred bag systems have gained in popularity and are being used in large numbers. The fact that stirred bags are more similar to the stainless steel reusable bioreactors, where there is extensive experience, has facilitated their penetration of the market and their integration into modern manufacturing processes.[3–5]

Single-use bioreactors are sterilized, ready-to-use, cultivation vessels. They are used once and then discarded after the end of the cultivation run. Processes based on single-use technology offer many

advantages. The use of such disposable systems eliminates the need for cleaning-in-place, sterilization-in-place, and cleaning validation. The risks of cross-contamination and production turnaround times are also reduced.[6] Further, single-use bioreactors reduce the validation time and shorten time to market,[3] which is an enormous advantage given the extensive development and increased demand of recombinant protein therapeutics. In 2013, estimates indicated that compared to stainless steel facilities, single-use operated facilities had annual production rates that were 27% greater and production costs that were 23% lower on a gram of mAb basis.[7]

In addition to the aforementioned advantages of single-use technology, we have proposed a new multichamber, single-use bioreactor that possesses additive advantages.[8] The proposed design involves chambers of different volumes, where a larger chamber encloses a smaller one, all presented as a single closed system that requires only one control unit and support structure. Thus, a 50- to 100-fold increase in the culture volume can be achieved in one single bag during the seed train process. That is a substantial enhancement to the current limit of only fivefold increase achievable in any stirred-tank single-use bioreactor on the market. The multichamber design allows a further reduction in the upstream processing costs. The cost reduction includes the cost associated with the purchase, qualification, and maintenance of equipment, as well as the cGMP factory footprint occupied by the different seed train bioreactors and control units. The design also reduces the risk of microbial contamination by allowing transfer of the cell culture between the different chambers, through internal tubing, via gravity or peristaltic pumps, without the need of opening the system. Our early proof of concept work[8] was based on a single-use, two-chamber bioreactor design. The smaller chamber had a 3 L maximum operating volume and had geometry similar to the Mobius® CellReady 3 L bioreactor, while the larger chamber had a 50 L maximum operating volume. The engineering characterization of the two chambers showed good agreement with other commercially available bioreactors with the same working volumes. However, the 50 L chamber required some design optimizations to improve the oxygen mass transfer (k_La) to be more in line with other bioreactors on the market.

The aim of the study presented here was to use computational fluid dynamics (CFD) simulations to model mixing and gassing in the 50 L chamber of the multichamber bioreactor and to validate the simulations with the published experimental data. The simulation model was then used to study the effect of different impeller and sparger sizes on k_La, as well as the effect of using a ring sparger instead of the pipe sparger, which was used in the early 50 L prototype.

CFD is a powerful tool that has been consistently applied to model stirred-tank bioreactors. The CFD models can generate high-resolution localized data regarding some parameters that are hard or even impossible to measure, such as the distributions of shear stress and turbulent kinetic energy.[9] Many scientific papers have used CFD to model fluid flow and turbulence inside agitated systems.[10–14] Other studies used CFD to model multiphase flow including gas phase, particle tracking or reaction processes.[15–21] The suitability of CFD models for engineering characterization of single-use bioreactors has also been demonstrated. Many case studies have been reviewed by Loffelholz et al.,[22] as well as some other recent studies.[23,24] These studies involved stirred-tank and wave-mixed bioreactors, as well as other bioreactor designs with uncommon mixing mechanisms like the oscillating disk with conical orifice in the Vibromix system and the air wheel in the PBS Biotech bioreactor. The case study of the PBS bioreactor was unique in the sense that the CFD simulations were used to develop the market-ready bioreactor based on only a prototype, which relates to one scope of this study regarding the multichamber bioreactor development. Applying CFD in the bioreactor development process led to a significant reduction in time and costs.[22] CFD has been also used to optimize cultivation and scale-up conditions in bioreactors by predicting the critical shear stress and hence proposing optimum impeller speeds for cell cultivation processes.[25,26]

In this study, numerical simulations were performed using ANSYS Fluent 17.0 (ANSYS Inc., Canonsburg, PA). An Eulerian–Eulerian model was used to model the multiphase flow combined with the *k-epsilon* dispersed turbulence model. A population balance model (PBM) has been previously used in multiphase simulations of stirred-tank reactors[27–29] and was used in this study to predict bubble size distribution in the stirred-tank reactor by considering bubble breakage and coalescence. The number and sizes of bins of the PBM for different agitation speeds were optimized by trial-and-error approach and were validated by experimental data generated from the 50 L chamber of the multichamber bioreactor. The model was then used to compare between a pipe sparger, which was used in the bioreactor prototype, and a ring sparger, in terms of the efficiency of oxygen mass transfer in the bioreactor. Oxygen mass transfer coefficient (k_La) is an indication of the oxygen transfer efficiency in the culture medium. A higher k_La value is required to ensure that the oxygen demand is met at higher cell densities, and to avoid excessive gassing which, in addition to the higher cost, may introduce excessive shear on the cells. Generally, while developing a new bioreactor, a design with a high (k_La) and a reasonable shear stress will enable growth of higher cell densities, reduce operating costs, and eventually result in a bioreactor that more favorably compares to commercially available top-tier bioreactors.

Different sparger and impeller sizes were also examined using the validated CFD model. Many studies, as reviewed by Markopoulos et al.,[30] have correlated k_La to the operating conditions like power input per unit volume (P/V) and superficial gas velocity for a given bioreactor geometry. In this study, we present a model equation to correlate k_La in a stirred-tank bioreactor to different geometrical and operating factors. The developed model equation correlates k_La to geometrical factors (i.e., impeller-to-vessel diameter ratio, D/T, and sparger-to-impeller diameter ratio, d_{sp}/D), mixing factors (i.e., Reynolds number, Re), and gassing factors (i.e., volumetric gas flow per unit liquid volume, Q/V_L). The developed model equation can be used to help the selection of the proper sparger, impeller, and vessel geometries and dimensions to be constructed and integrated during the development process of stirred-tank bioreactors, especially the next generation multichamber bioreactor prototypes of different operating volumes. The model can also be used to predict the oxygen mass transfer efficiency in stirred-tank bioreactors under variable operating conditions.

2 | BIOREACTOR GEOMETRY RECONSTRUCTION AND MESH REGENERATION

The bioreactor under consideration was the 50 L chamber of the two-chamber, single-use bioreactor described earlier (Figure 1a).[8] The chamber was a cylindrical vessel with a diameter (T) of 38.0 cm and a height of 67.0 cm. The liquid height at the maximum working volume was 42.0 cm which was the height considered in the CFD model. A three-blade impeller pitched at 30° was carried on a central, top mounted shaft and was used to mix the fluid inside the bioreactor. The impeller diameter (D) was 22.8 cm. The air sparger was placed at the bottom center of the bioreactor. The sparger was a pipe with a length of 3.1 cm and constant pore sizes (d_h) of 10 μm. For CFD simulations, different impeller diameters were examined, as well as other pipe spargers of different lengths and ring spargers with variable diameters. Experiments and simulations were performed at impeller tip speeds of 0.6, 1.2, and 1.8 m/s, which for the constructed prototype, corresponded to 50, 100, and 150 rpm, respectively. The air sparging rate was set at 0.02, 0.05, and 0.10 volume of air per volume of liquid per minute (VVM).

Booleans for the solid parts of the bioreactor (i.e., shaft, impeller, and sparger) were created so that only the fluid domains of the bioreactor were considered for the simulation. Two distinct fluid domains were created. A smaller domain, or the multireference frame (MRF), was defined near the impeller and was set as a rotating region with a velocity corresponding to the impeller tip speed. The other volume, which was the stationary volume, was the volume away from the impeller.

Unstructured tetrahedral meshes were generated using ANSYS Meshing (ANSYS Inc., Canonsburg, PA). Interfaces were defined at the joint boundaries of the two fluid domains allowing free flow across the two regions. The ANSYS meshing tool generated unstructured grids consisting of tetrahedral elements (Figure 1b). Mesh quality has been improved and checked to meet the requirement in ANSYS Fluent. Specifically, all mesh elements had skewness less than 0.83, and 98.4% of the elements had an aspect ratio between 1 and 2. A mesh independence test was performed to identify the optimum number of mesh elements that provides accurate results and good computational efficiency. Multiple sets of mesh with different numbers of elements were generated and simulations were run on each of them. The results were initially found to vary with the mesh element size until it reached a certain point where the results were constant and no longer dependent on the grid size. The k_La value was the parameter selected to perform the mesh independence test. As shown in Figure 2, increasing the number of mesh elements beyond 1.48 million cells resulted in negligible differences in k_La values, and thus the 1.48 million-grid size was selected for all further simulations. For the mesh independence test, simulations were run at the bioreactor impeller speed of 150 rpm and an inlet airflow rate of 0.1 VVM. The final mesh (shown in Figure 1) contains 1,487,040 elements and 266,038 nodes.

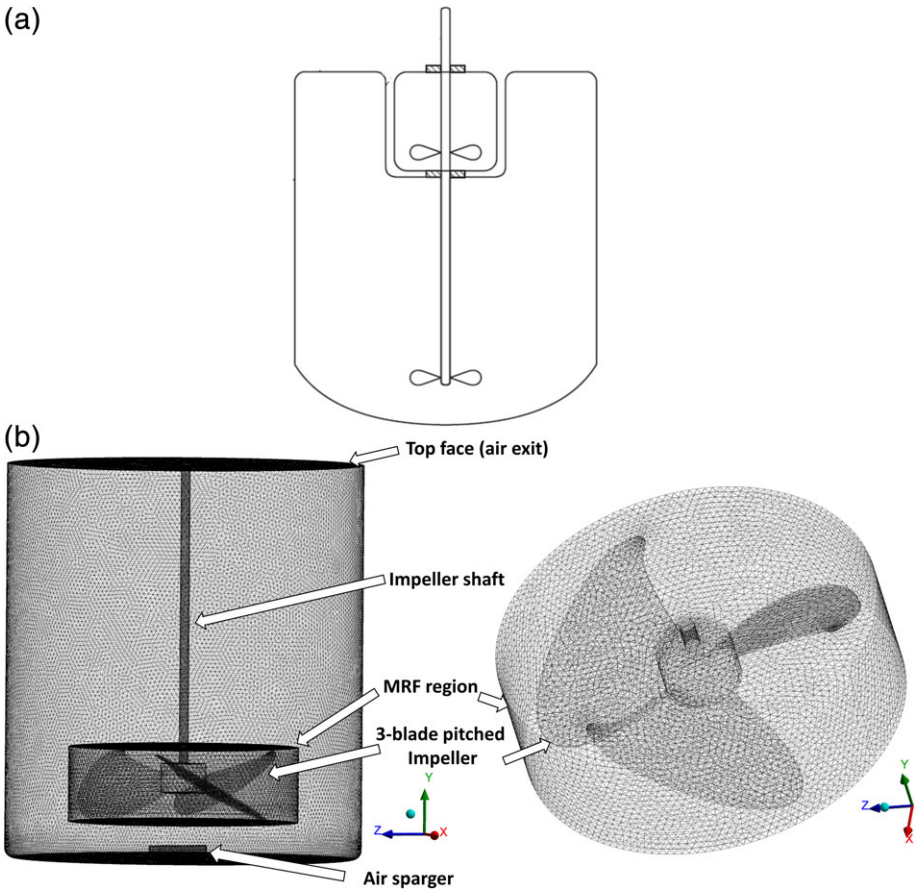

FIGURE 1 (a) A schematic diagram for the multi-chamber bioreactor, (b) illustration of the 50 L chamber geometry and mesh

3 | NUMERICAL SETUP

The CFD simulations were carried out using the ANSYS FLUENT 17.0 finite volume solver. The bioreactor vessel containing liquid mixed by an impeller and aerated from the bottom was represented by a multiphase gas–liquid system. The system was modeled using the Eulerian–Eulerian multiphase model, where water was the primary phase and air was the secondary phase and was dispersed in water as a continuous phase as air bubbles.

All walls were treated with no-slip boundary conditions. The sparger surface was treated as air velocity inlet, where the air volume fraction was set to unity. The bioreactor top was set as a degassing outlet to allow only air to escape from the bioreactor top boundary and not water. Properties of fluids in the simulations were set as follows: for water, ρ_L = 998.2 kg/m^3, μ_L = 0.001 kg/m/s, while for air ρ_G = 1.225 kg/m^3, $\mu_G = 1.789 \times 10^{-5}$ kg/m/s, and the water-air interfacial tension σ_L = 0.072 N/m.

The phase-coupled SIMPLE algorithm was used for pressure velocity coupling. The second order upwind scheme was used for momentum discretization, and the first order upwind scheme was used for the turbulent kinetic energy (k) and turbulent dissipation rate (ε). QUICK scheme was used to solve for volume fraction while the Green-Gauss node-based method was used for gradient. For each simulation, single-phase flow was performed first by solving continuity and momentum equations. The single-phase solution was then used to initialize the multiphase solution. The time step was set to 0.01 s in single-phase simulations and 0.001 s in multiphase simulations. The maximum number of iterations per time step was set to 60. Convergence was determined by reaching residuals below 1×10^{-5} for all parameters and 1×10^{-4} for continuity and by reaching a constant k_La value over a significant number of time steps.

4 | GOVERNING EQUATIONS

4.1 | Eulerian–Eulerian multiphase model

This model involves solving the Navier–Stokes equations assuming constant density and viscosity for both phases. The governing equations for mass and momentum conservation can be written as follows:

$$\frac{\partial}{\partial t}(\rho_i \alpha_i) + \nabla.(\alpha_i \rho_i \boldsymbol{U_i}) = 0 \tag{1}$$

$$\frac{\partial}{\partial t}(\rho_i \alpha_i \boldsymbol{U_i}) + \nabla.(\rho_i \alpha_i \boldsymbol{U_i U_i}) = -\alpha_i \nabla p + \nabla.\boldsymbol{\tau_{ef}} + \boldsymbol{R_i} + \boldsymbol{F_i} + \alpha_i \rho_i \mathbf{g} \tag{2}$$

where ρ_i, α_i, and $\boldsymbol{U_i}$ are the density, volume fraction, and mean velocity vector of phase i, respectively, where the subscript i refers to either the liquid (L) or gas (G) phase. The terms p, $\boldsymbol{R_i}$, and $\boldsymbol{F_i}$ represent the pressure, momentum exchange, and centrifugal forces. The term $\mathbf{g}$ is acceleration due to gravity. The Reynolds stress tensor, denoted by $\boldsymbol{\tau_{ef}}$, was described by the k-ε turbulence model provided by FLUENT and was used with default settings.[31]

The sum of both liquid and gas phase volume fractions remains unity in every cell domain as follows:

$$\alpha_L + \alpha_G = 1 \tag{3}$$

The drag force acting on the air bubbles resulting from the relative velocity between the two phases is the most important interface force and can be described as follows:[32]

Drag force for the secondary phase:

$$\boldsymbol{R_G^{Drag}} = \frac{18\alpha_G(1-\alpha_G)\mu_L C_D \mathrm{Re}_p}{24 d_p^2}(\boldsymbol{U_G} - \boldsymbol{U_L}) \tag{4}$$

Drag force for primary phase:

$$\boldsymbol{R_L^{Drag}} = -\boldsymbol{R_G^{Drag}} \tag{5}$$

While there are several drag law models provided by FLUENT, Kaiser[33] reported that the drag coefficients, C_D, predicted from nine different models were nearly identical at low particle Reynolds number, Re_p, and the drag coefficients only began to deviate when Re_p was close to 1,000. In our study, the maximum Re_p was 0.22, as calculated from Equation 7, which suggests that any of the drag law models can be used in our simulations with little concern of differences. The drag coefficient described by the Schiller and Naumann correlation[32] is frequently used in literature to simulate stirred-tank bioreactors,[27,28,34] and was selected in our study:

$$C_D = \begin{cases} \dfrac{24\left(1 + 0.15\,\mathrm{Re}_p^{0.687}\right)}{\mathrm{Re}_p} & \mathrm{Re}_p \le 1000 \\ 0.44 & \mathrm{Re}_p > 1000 \end{cases} \tag{6}$$

The particle Reynolds number [35]:

$$\mathrm{Re}_p = \frac{\rho_L |\boldsymbol{U_G} - \boldsymbol{U_L}| d_p}{\mu_L} \tag{7}$$

4.2 | Turbulence model

Because the volume fraction and the density of the secondary phase are low, and the density difference between the two phases is high, the dispersed k-ε turbulence model was used. In this dispersed k-ε model, the turbulence of dispersed phase is not considered, and the flow of this secondary phase is considered to be laminar.[36]

The liquid phase turbulence viscosity is described as:[37]

$$\mu_{t,L} = \rho_L C_\mu \frac{k_{Liq}^2}{\varepsilon_L} \tag{8}$$

where the turbulent kinetic energy term for the liquid phase (k_{Liq}) should not be confused with the convective mass transfer coefficient (k_L), that is, a part of the oxygen mass transfer coefficient (k_La). Within

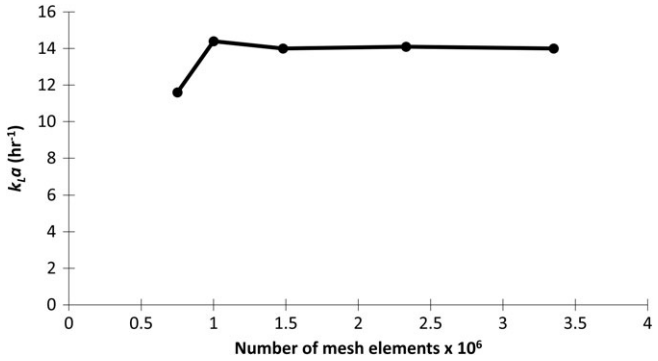

FIGURE 2 Mesh independence test where k_La is plotted as a function of number of mesh elements. Simulations are performed at impeller tip speed of 1.8 m/s and aeration rate of 0.1 VVM

Equation 8, the transport equations for the turbulent kinetic energy, k, and the turbulent energy dissipation, ε, are given by:

$$\frac{\partial(\rho_L\alpha_L k_{Liq})}{\partial t} + \nabla.(\rho_L\alpha_L k_{Liq}\boldsymbol{U_L}) = \nabla.\left(\alpha_L\frac{\mu_{t,L}}{\sigma_k}\nabla k_{Liq}\right) + \alpha_L G_{kL} - \alpha_L\rho_L\varepsilon_L + \alpha_L\rho_L\prod_{kL} \quad (9)$$

$$\frac{\partial(\rho_L\alpha_L\varepsilon_L)}{\partial t} + \nabla.(\rho_L\alpha_L\varepsilon_L\boldsymbol{U_L}) = \nabla.\left(\alpha_L\frac{\mu_{t,L}}{\sigma_\varepsilon}\nabla\varepsilon_L\right) + \alpha_L\frac{\varepsilon_L}{k_{Liq}}(C_{1\varepsilon}G_{kL} - C_{2\varepsilon}\rho_L\varepsilon_L) + \alpha_L\rho_L\prod_{\varepsilon L} \quad (10)$$

where G_{kL} is the rate of production of k, $\prod_{kL}$, and $\prod_{\varepsilon L}$ account for the influence of dispersed phase on the continuous phase,[38] while C_μ, $C_{1\varepsilon}$, $C_{2\varepsilon}$, σ_k, and σ_ε are model parameters given the values 0.09, 1.44, 1.92, 1.0, and 1.3, respectively.[31]

4.3 | Population balance model

While constant bubble size models are simple and require less computational time, they do not accurately represent the physical system.[37,39] Bubbles are discharged from the sparger with a uniform diameter. Once they are in the medium, however, the bubbles interact with the moving primary phase and undergo breakup and coalescence. Bubble breakup occurs when the liquid disruptive forces overcome the bubble surface tension, while coalescence happens when bubbles collide strongly enough to break the bubble thin film. A PBM provides more information that is accurate by predicting coalescence and breakup mechanisms and providing information on the bubble size and the bubble size distribution within the bioreactor.[39–41] In this study, the method of classes (discrete method)[42,43] was used for discretizing and solving the population balance partial differential equation, which can be written as follows:

$$\frac{\partial(\rho_G n_i)}{\partial t} + \nabla.(\rho_G\boldsymbol{U_{G,}}_i n_i) = \rho_G(B_{iC} - D_{iC} + B_{iB} - D_{iB}) \quad (11)$$

In this equation, n_i is the number of bubbles in the bubble class i, $U_{G,\,i}$ is the velocity vector of gas phase bubbles in the class i, B_{iB} and B_{iC} are the bubble birth rates due to breakage and coalescence, and D_{iB} and D_{iC} are the bubble death rates due to breakage and coalescence, respectively. These terms are modelled as functions of bubble volumes V'as follows:[42]

$$B_{iC} = \frac{1}{2}\int_0^V a(V-V',V')n(V-V',t)n(V',t)dV' \quad (12)$$

$$D_{iC} = \int_0^\alpha a(V,V')n(V,t)n(V',t)dV' \quad (13)$$

$$B_{iB} = \int_V^\alpha m(V')b(V')p(V,V')n(V',t)dV' \quad (14)$$

$$D_{iB} = b(V)n(V,t) \quad (15)$$

In these equations, $a(V, V')$ is the coalescence rate between the different sized bubbles of volumes V and V', $b(V')$ is the breakage rate of bubble with volume V', $m(V')$ is the number of daughter bubbles formed due to fragmentation from bubbles of volume V'. $n(V, t)$ is the number of bubbles of volume V at time t, and $p(V, V')$ is the probability density function to determine offspring bubbles of volume V generated from bubbles of volume V'.

Because it is more useful to work in terms of the volume fraction of a particular bin of bubbles (f_i) than the number of bubbles in that bin (n_i), it is convenient to express Equation 11 in different terms. With the volume fraction of bubble size i defined as

$$\alpha_i = n_i V_i \quad (16)$$

and f_i defined as the ratio of the volume fraction of the i^{th} bin to the total gas volume fraction,

$$f_i = \frac{\alpha_i}{\alpha_G} \quad (17)$$

and

$$\sum_i f_i = 1 \quad (18)$$

The population balance equation (Equation 11) can be written in terms of f_i and α_G:

$$\frac{\partial(\rho_G f_i\alpha_G)}{\partial t} + \nabla.(\rho_G\boldsymbol{U_{G,}}_i f_i\alpha_G) = \rho_G V_i(B_{iC} - D_{iC} + B_{iB} - D_{iB}) \quad (19)$$

Sauter mean diameter (d_{32}) was used as the input bubble diameter in the simulation and was used to couple the PBM with the fluid dynamics.[42] The Sauter mean diameter is given by

$$d_{32} = \frac{\sum n_i d_i^3}{\sum n_i d_i^2} \quad (20)$$

Many breakage and coalescence models for bubble flow are available. These models, however, are quite similar with some minor

differences in the model constants or assumptions used to develop the model.[15] While the discussion of aggregation and breakage kernels is beyond the scope of this article, it is worth mentioning that several studies[44–47] have detailed comparisons between the different breakage and coalescence models, including those proposed by Prince and Blanch[48], Luo and Svendsen[49], Luo[50], Chesters[51], Martínez-Bazán et al.[52], Alopaeus et al.[53], and Lehr et al.[54] The findings from these studies suggest that there is little difference between the mean flow, gas hold-up and bubble Sauter mean diameter predicted by the different models, while there is some difference in the predicted bubble size distribution.

In this study, The FLUENT embedded Luo-Svendsen[49] and Luo[50] models were used to model both the breakage and coalescence of bubbles, respectively. The models have been frequently used in literature to simulate stirred-tank bioreactors using FLUENT software.[27,28] In the breakage model, only turbulent eddies with a scale smaller than the bubble diameter are considered to cause the bubbles to break while larger scale eddies are only considered to convect the bubbles.

4.4 | Mass transfer coefficients and bubble diameter

The models used by Rathore et al.[27] were based on Higbie's penetration theory[55] and were used to theoretically estimate the mass transfer coefficient (k_L) and the interfacial area available for mass transfer (a) as follows:

$$k_L = \frac{2}{\pi}\sqrt{D_{O_2}}\left(\frac{\varepsilon\rho_L}{\mu_L}\right)^{\frac{1}{4}} \quad (21)$$

$$a = \frac{6\alpha_G}{d_{32}} \quad (22)$$

where D_{O_2} is the molecular diffusivity of oxygen and is equal to 1.97×10^{-9} m^2/s.[40] Both models were used as user defined functions in FLUENT to predict k_La.

The original diameter (d_p) of the bubbles coming out from the sparger holes of diameter d_h was modeled by:[48,56]

$$d_p = \left(\frac{6\alpha d_h}{g(\rho_L - \rho_G)}\right)^{1/3} \quad (23)$$

The oxygen mass transfer coefficient k_La was experimentally determined by the gassing out method as previously described for the 50 L chamber of the multichamber single-use bioreactor.[8]

5 | STATISTICAL ANALYSIS AND CORRELATION EQUATION

A randomized response surface method was applied to study the effect on k_La of the sparger-to-impeller diameter ratio (d_{sp}/D), impeller-to-vessel diameter ratio (D/T), Reynolds number (Re), and the gas flow rate per unit liquid volume (Q/V_L). The simulation results used in the analysis were performed at d_{sp}/D ratios: 0.086, 0.173, 0.259, 0.500, and 0.800; D/T ratios: 0.2, 0.4, and 0.6; Re numbers within the range 20,000–100,000; and Q/V_L: 1.2, 3.0, and 6.0 L of gas/ L of liquid/hour. A total of 16 simulation results at different levels of the four studied factors were evaluated by an analysis of variance (ANOVA) statistical test. A quadratic model equation was generated to correlate the test factors to k_La values. All data were analyzed using Design-Expert 11.

6 | RESULTS AND DISCUSSION

6.1 | Single-phase flow pattern

As shown in Figure 3, the velocity contours and vectors show the flow pattern at a mid-plane of the 50 L bioreactor. The fluid is discharged from the impeller tip toward the vessel wall. As the fluid hits the wall, it is divided into two loops that recirculate at the top and the bottom of the stirrer. This flow pattern is consistent with what was simulated in the Mobius® CellReady bioreactor with a similar three-blade pitched impeller.[24,34] These flow simulations were validated by Particle Image Velocimetry (PIV)[24] and by visual observation of the trajectory of small plastic particles suspended in the bioreactor.[34] The highest velocity magnitude was shown at the closest proximity to the impeller tip and the velocity gradient migrated away from the tip and across the boundary between moving reference frame and the stationary domain, thus reflecting what we know to be representative of the physical system. This observation was true for all the three tip speeds tested. The top circulation loop showed lower velocities than the lower loop, which was also consistent with what was previously reported for the Mobius® CellReady bioreactor.

6.2 | Multiphase fluid simulation and k_La prediction

Although assuming a constant bubble diameter throughout the bioreactor operation saves computational effort and has been successfully used in some studies,[34,57] our k_La prediction from a constant bubble size simulation was substantially different from the experimental results. At 0.6 impeller tip speed and 0.1 VVM, the experimental k_La measurement was 7.3/hr while the k_La predicted from the constant bubble size simulation was 18.2/hr. The PBM simulation, with bin sizes displayed in Table 1, predicts a more realistic k_La value of 8.0/hr.

6.2.1 | Model validation and optimization of bin sizes

The agitation speed and aeration rate are expected to affect the bubble size and bubble size distribution within the bioreactor, and a single PBM model is incapable of accurately predicting the bubble size and size distribution at all of these operating conditions. In our study, therefore, the number and sizes of bins were optimized for the different operating conditions using a trial-and-error method as has been reported by Sarkar et al.[28] For each impeller tip speed, a different number of bins of different bubble diameters were tried, and the PBM

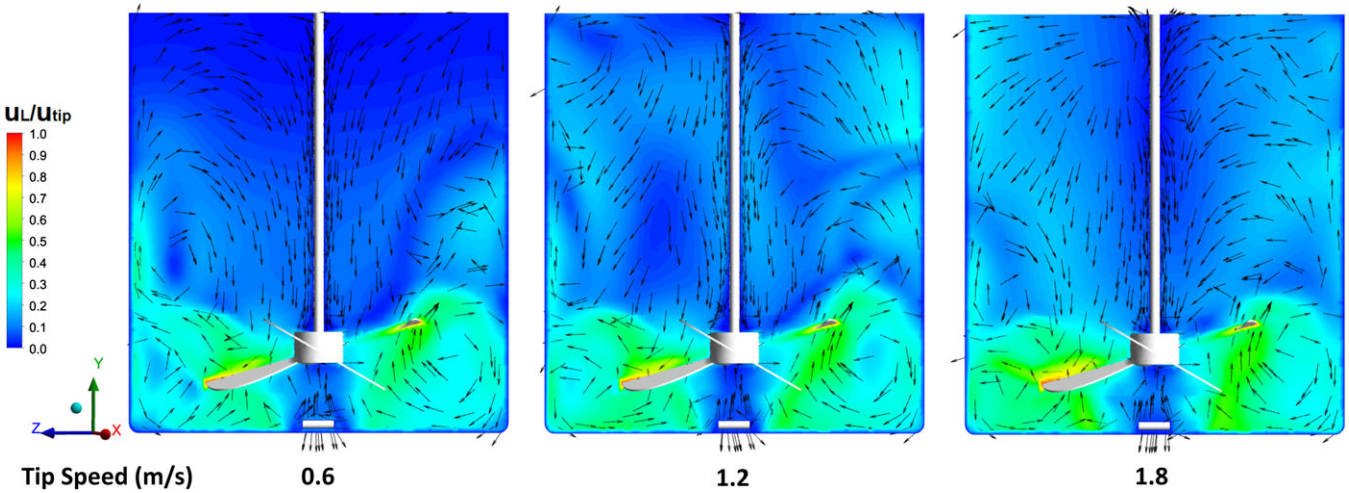

FIGURE 3 Contours and vector plots of fluid velocity in a single-phase flow at different impeller tip speeds. Velocity of liquid (U_L) is shown normalized to the tip speed (U_{tip})

model was validated by predicting k_La values within 10% deviation from the experimental results at various tip speeds and aeration rates, as shown in Figure 4. Table 1 shows the optimized bin number and sizes at different impeller tip speeds, where the original bubble diameter emerging from the sparger predicted from Equation 23 was always set as the middle bin allowing for equal chances of breakage and coalescence in both larger and smaller bins. While the bubble diameter predicted from Equation 23 was 0.88 mm, the Sauter mean diameter predicted from the PBM simulations was always larger than 0.88 mm, which indicated that coalescence dominated over breakage.

The CFD model described above was then used to explore the effect of different design parameters on the k_La for the sake of optimizing the bioreactor design. Not all of the following simulations were experimentally validated.

TABLE 1 Number and size of bins used in the population balance model to simulate the multiphase flow at different impeller tip speeds

Tip speed (m/s)	1.8	1.2	0.6
	Bin bubble diameter (mm)		
Bin-0	7.04	2.66	1.88
Bin-1	4.98	2.02	1.46
Bin-2	3.52	1.53	1.13
Bin-3	2.49	1.16	0.88
Bin-4	1.76	0.88	0.68
Bin-5	1.24	0.67	0.53
Bin-6	0.88	0.50	0.41
Bin-7	0.62	0.38	
Bin-8	0.44	0.29	
Bin-9	0.31		
Bin-10	0.22		
Bin-11	0.16		
Bin-12	0.11		

6.2.2 | Effect of sparger shape on k_La

Pipe spargers resulted in approximately 30% lower k_La values than the ring spargers of the same surface area, as shown in Figure 5a, where simulations were run at an impeller tip speed of 1.2 m/s and an aeration rate of 0.1 VVM. A higher gas volume fraction was observed with the ring sparger simulations, as shown in Figure 5b, which can be attributed to the fact that the ring sparger configuration produces more bubbles at a closer proximity to the impeller tip. The fluid at the impeller tip experiences higher turbulence and better distribution across the bioreactor vessel, which can be observed from the top view of the vessel showing dispersed gas (Figure 6). In agreement with the simulation results, a previous experimental study showed similar results.[58] The study showed higher gas hold-up with the ring sparger compared to the pipe sparger over a wide range of impeller speeds and gas velocities. Lower impeller speeds showed 25% improvement in gas hold-up with the ring sparger and 18% improvement at higher impeller speeds.

6.2.3 | Effect of sparger size on k_La

Different sizes of spargers were tested to examine the effect of the sparger size on k_La. Simulations were run at a stirrer tip speed of 1.2 m/s and a gassing rate of 0.1 VVM. As shown in Figure 7a, better k_La values were achieved by increasing the sparger size until some point where the use of bigger spargers led to a sharp drop in k_La. The trend of the k_La values with increased sparger size was consistent with the trend of the volume fraction of air (Figure 7b). The best k_La value was achieved when the ratio between the sparger diameter and the impeller diameter (d_{sp}/D) was 0.8. At this d_{sp}/D ratio, a 16% increase in the k_La value was observed over the smallest sparger size tested, which had a d_{sp}/D ratio of 0.086. A sharp reduction of 43% in k_La was observed when the d_{sp}/D was increased from 0.8 to 1.0. The air bubble size distribution at a midplane of the bioreactor is shown in Figure 8, where it can be

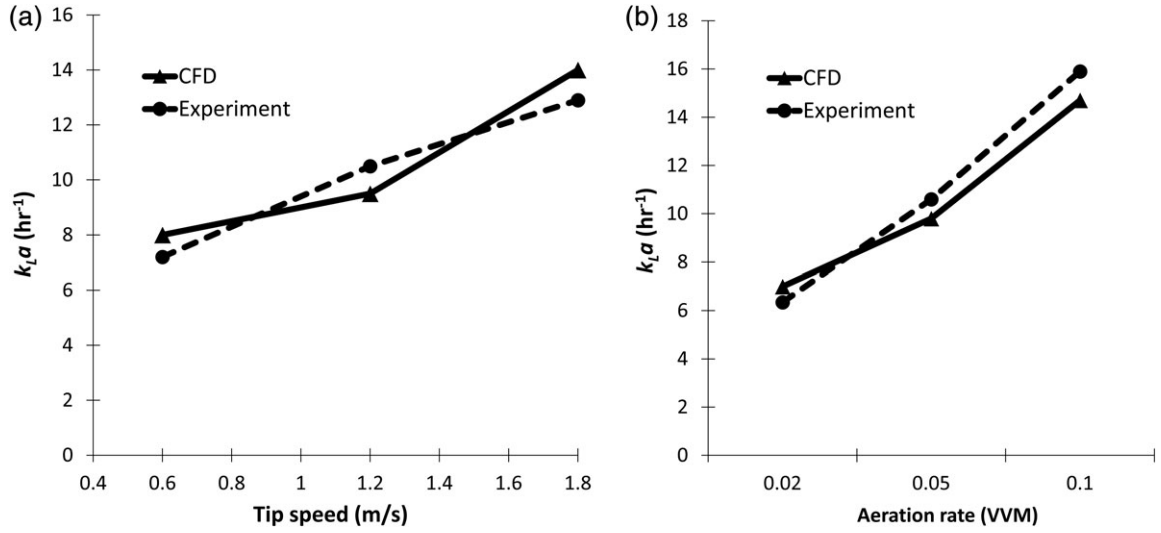

FIGURE 4 PBM model validation. (a) Validation versus k_La experimental data obtained at different impeller tip speeds and a constant aeration rate of 0.1 VVM, (b) validation versus k_La experimental data obtained at different aeration rates and a constant impeller tip speed of 1.8 m/s

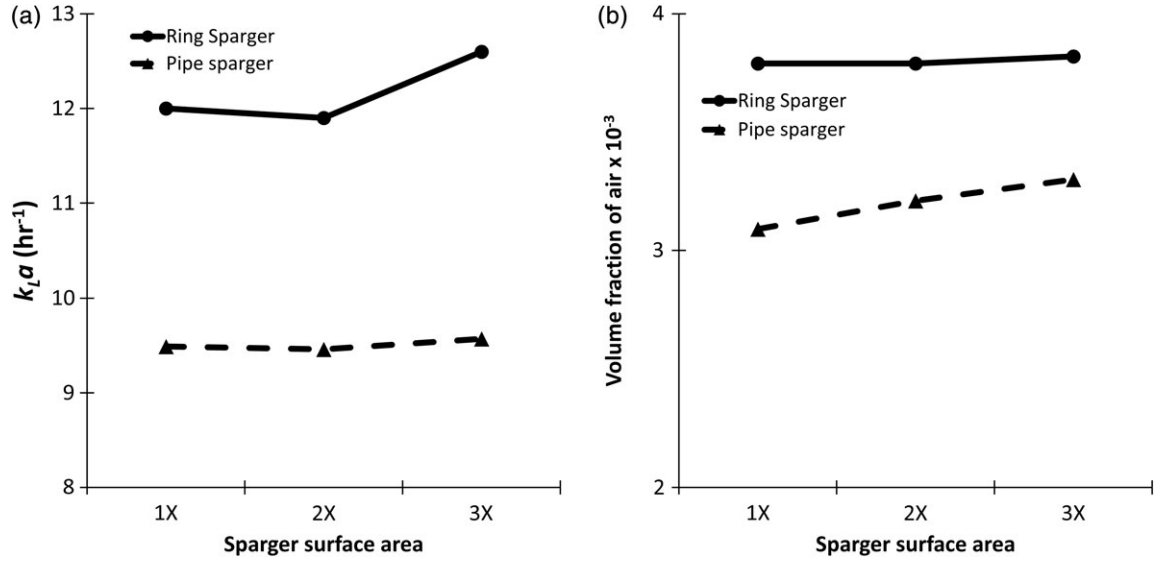

FIGURE 5 Comparison between pipe and ring spargers of same sparging surface area, at impeller tip speed of 1.2 m/s and gassing rate of 0.1 VVM (1X is equivalent to the surface area of the sparger used in the prototype). (a) Effect of sparger geometry on *kLa*, (b) effect of sparger geometry on air volume fraction

observed that at the small sparger diameter, the air bubbles are purged toward the center of the vessel where the fluid velocity and turbulence is low. The bubbles are thus prone to coalesce and to escape the vessel quickly from top. In the best case, the sparger diameter to the impeller diameter ratio was equal to 0.8, and a fraction of the bubbles is shown to be forced toward the impeller tip where the velocity and turbulence are at their maximum, thus causing the bubbles to break. The smaller bubbles are thrown toward the vessel wall and residence time of the bubbles inside bioreactor is increased. A fraction of the bubbles is also pushed towards the center of the vessel, where they coalesce and rise upward. This combination of events allows a better distribution of gas inside the vessel, which is reflected in the higher gas volume fraction. In contrast, at a sparger diameter that is equivalent to the impeller diameter, the gas bubbles are mostly dispersed outward by the impeller and are not efficiently distributed in the center of the vessel. That poor distribution of gas bubbles inside the bioreactor leads to a lower gas volume fraction and hence, a lower k_La. The simulation results are supported by experimental results reported by Rewatkar et al.[58] where a ring sparger of a diameter that is 0.8 of the impeller diameter showed a higher gas hold-up over a wide range of impeller speeds compared to other ring spargers with a diameter that was either half or equal to the diameter of the impeller. The d_{sp}/D ratio of 0.8 was also recommended by McFarlane et al.[59] to enhance gas handling capability and energy efficiency in dispersing gas in stirred-tank bioreactors. Birch and Ahmed[60] also showed that the gas hold-up dropped significantly when the diameter of the ring sparger exceeded the diameter of the impeller.

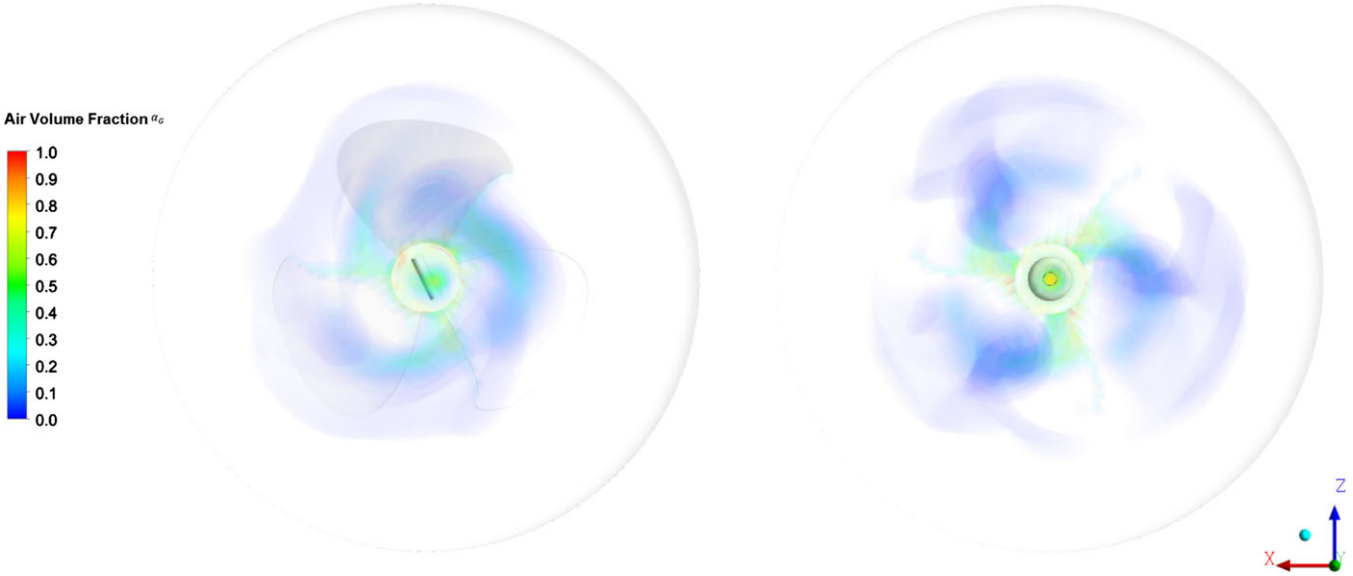

FIGURE 6 Top view of the air volume fraction inside the bioreactor with a pipe sparger (left) and a ring sparger (right)

6.2.4 | Effect of impeller diameter on k_La

A number of studies, reviewed by Markpoulos et al.,[30] correlated k_La to the power input per unit volume (P/V), which was directly proportional to the fifth power of the impeller diameter according to the following equation:

$$P/V = \frac{N_e \cdot \rho \cdot n^3 \cdot D^5}{V} \quad (24)$$

In contrast, García-Cortés et al.[61] reported a correlation where k_La was directly proportional to the impeller-to-vessel diameter (D/T) ratio raised to the power of 2.8. In the present study, simulations were consistent with the aforementioned findings in the sense that the larger impeller diameter produced higher k_La values. For a constant d_{sp}/D ratio of 0.8, the k_La value at a 0.6 D/T ratio was higher than at a 0.4 D/T ratio by more than 60% and was more than double compared to a D/T ratio of 0.2 (Figure 9). The mid-plane contours of the gas volume fraction (Figure 10) show a clear enhancement in gas distribution inside the vessel with increasing impeller diameter. The better gas distribution can be related to the enhanced mixing behavior, where a larger impeller-to-vessel diameter ratio has been reported to enhance mixing behavior with any type of agitator.[62]

6.3 | Statistical analysis and model equation

The ANOVA test results were helpful to evaluate the accuracy of the applied model. A correlation coefficient (R^2) of 0.9650, which was quite close to the adjusted R^2 value of 0.9417, indicated that the

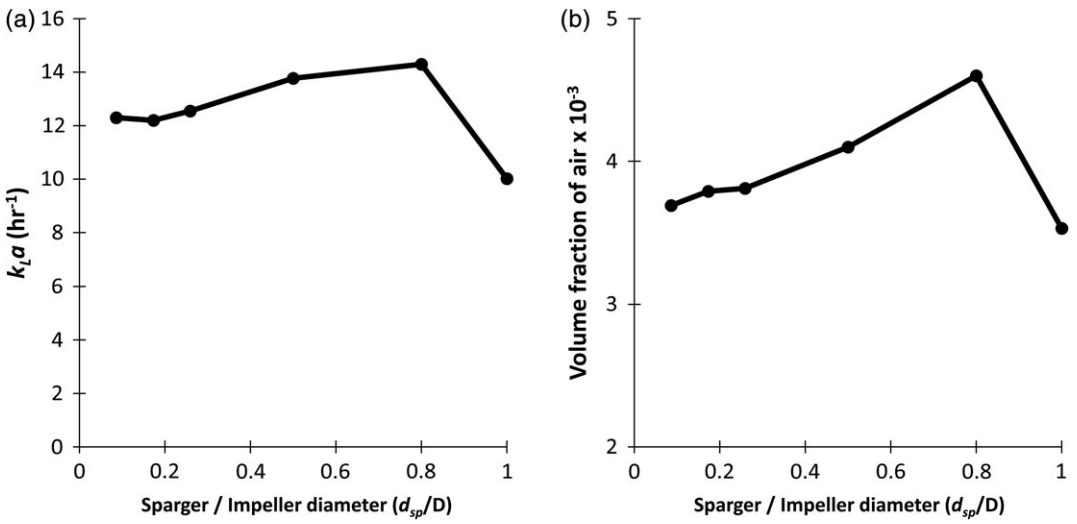

FIGURE 7 Effect of ring sparger diameter on (a) *kLa* and (b) air volume fraction. Simulations were performed at an impeller tip speed of 1.2 m/s and gassing rate of 0.1 VVM

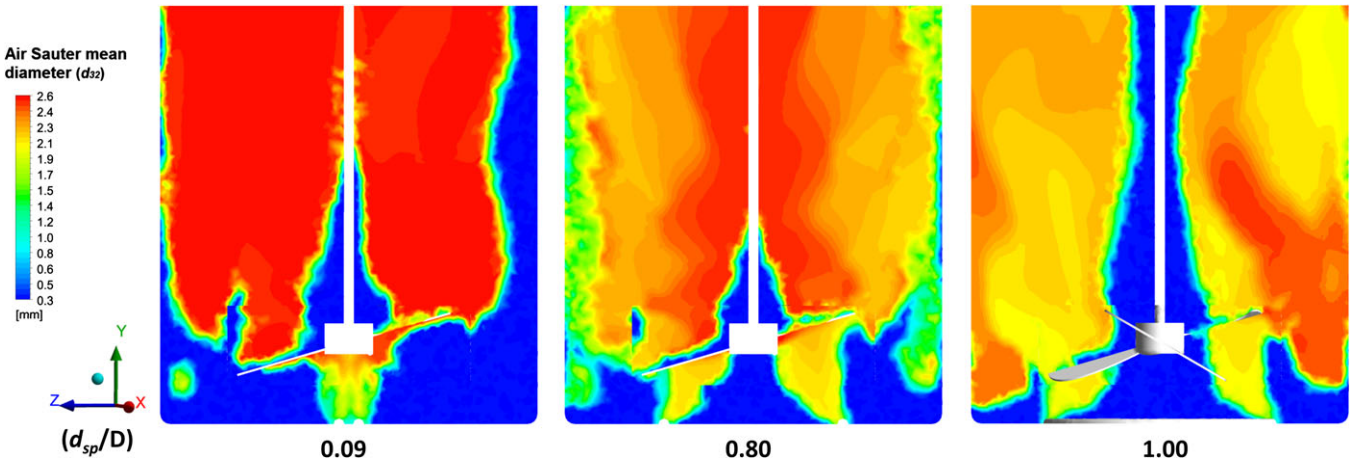

FIGURE 8 Contour plots of bubble size distribution at d_{sp}/D ratio of 0.09 (left), 0.8 (middle), and 1.0 (right). Simulations were performed at an impeller tip speed of 1.2 m/s and gassing rate of 0.1 VVM

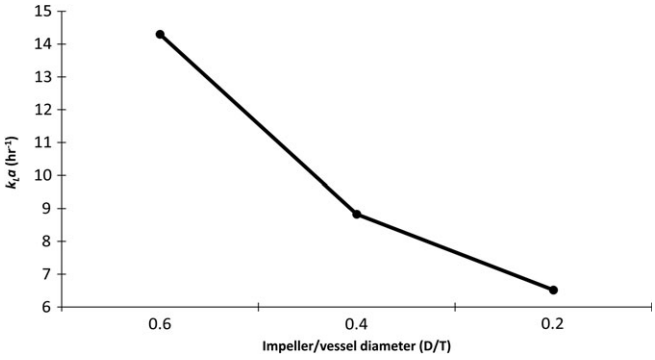

FIGURE 9 Effect of impeller diameter to vessel diameter ratio (D/T) on k_La

model showed a true relationship between the response and the independent variables within the tested range.

A predicted R^2 of 0.8896, with less than 0.2 difference from the adjusted R^2 (as suggested by the Design-Expert Software), as well as a good fit between simulation results and the model predictions, shown in Figure 11a, indicated that the model is a good predictor. The small standard deviation (0.845) revealed the reproducibility of the model, and the small *p*-value (<0.0001) indicated that the model is highly significant. Contour line maps, shown in Figure 11(b–g), show the effect of every two tested variables on the response (k_La). The final model equation correlates k_La to the four tested factors within the ranges commonly used in cell culture applications and can be written as:

$$k_La = -7.4353 + 0.102752\,(\mathrm{Re}) - 16.86911\left(\frac{D}{T}\right) + 12.6307\left(\frac{d_{sp}}{D}\right) + 1.61915\left(\frac{Q}{V_L}\right) + 32.10674\left(\frac{D}{T}\right)^2 - 11.4995\left(\frac{d_{sp}}{D}\right)^2 \quad (25)$$

Based on the above model analysis, the response surface model was suitable for correlating k_La to both geometrical and operating parameters and thus can be used to predict k_La in stirred-tank bioreactors and to optimize the bioreactor geometry and operating conditions.

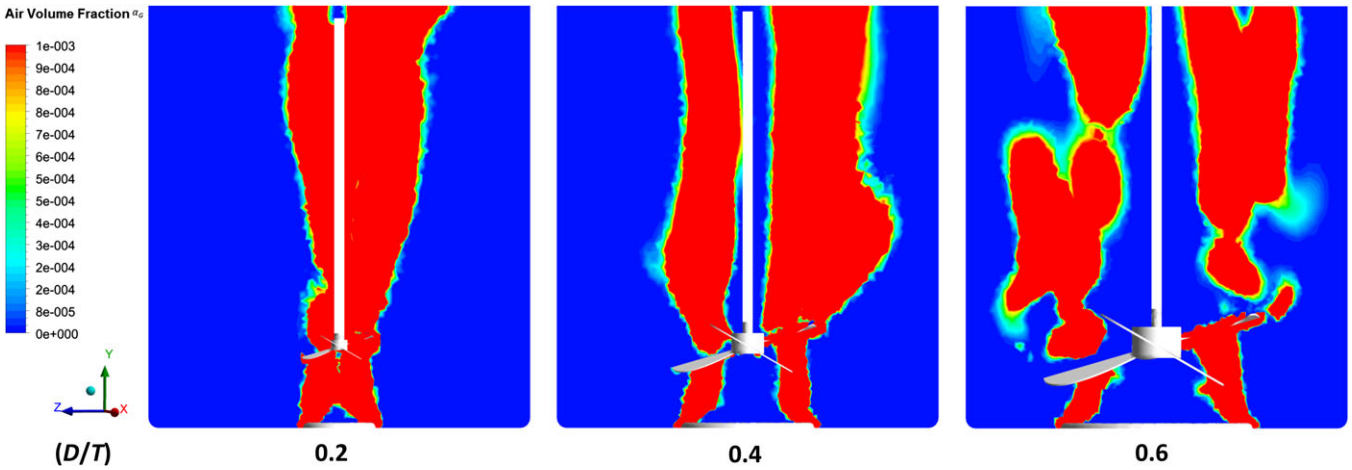

FIGURE 10 Contours of air volume fraction (αG) at the bioreactor mid-plane with different impeller diameters (D/T = 0.2, 0.4, and 0.6). In all cases d_{sp}/D is 0.8, the tip speed is 1.2 m/s, and the aeration rate is 0.1 VVM

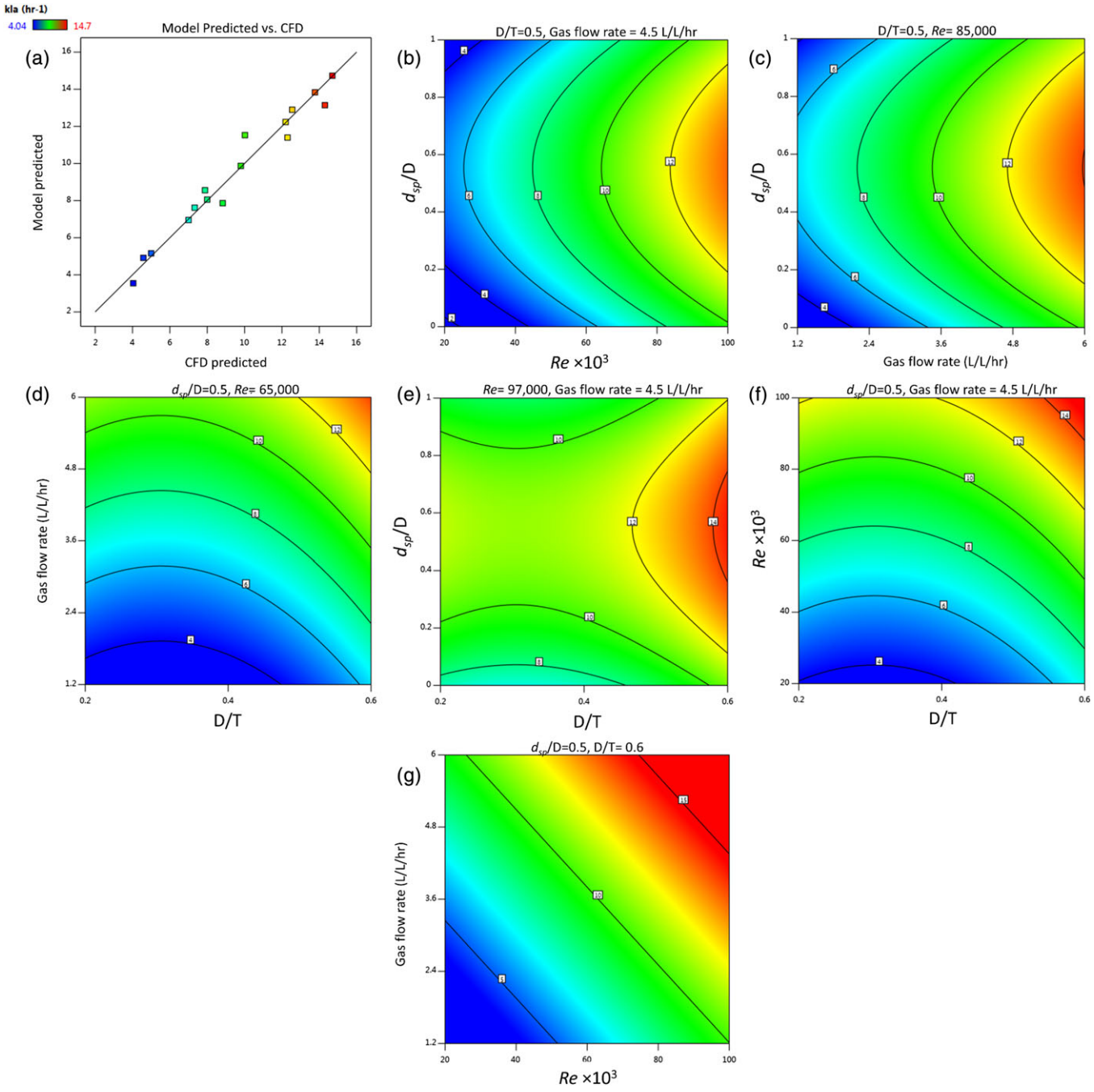

FIGURE 11 (a) Linear plot of model predicted versus CFD predicted k_La values. (b–g) Contour line maps showing the effect of different variables d_{sp}/D, D/T, *Re*, and gas flow rate on k_La

7 | CONCLUSIONS

High efficiency of oxygen mass transfer in a bioreactor is essential for a successful cell culture process. Oxygen mass transfer coefficient (k_La) is a widely used parameter to evaluate the design and performance of a bioreactor. Over the course of designing a new bioreactor, an exceedingly large number of combinations of different geometries and operating conditions may be required to be evaluated, which makes the experimental evaluation of all possible configurations almost impossible. Thus, CFD is a powerful tool that has been often recruited to help design and optimize bioreactor performance, requiring less time and fewer experiments.

In this study, we presented a CFD model to predict k_La in a stirred-tank bioreactor for mammalian cell culture, and the model was validated by experimental k_La measurements. A PBM that accounted for air bubble coalescence and breakup was shown to be essential for an accurate prediction of the multiphase flow inside the bioreactor. The validated CFD model was used to study the effect on k_La of various sparger geometries and sizes, as well as different impeller sizes. A ring sparger was shown to exhibit a superior

performance over the pipe sparger in terms of k_La and gas hold-up, with an optimum diameter that is 80% of the impeller diameter. Reducing the impeller diameter was also shown to decrease k_La inside the stirred-tank bioreactor. The CFD model was also used to develop a formula to correlate k_La to sparger size, impeller size, and mixing and gassing conditions. While k_La has been a primary factor in evaluating stirred-tank bioreactors, existing literature only correlates k_La to the operating conditions and a geometry that is assumed to be fixed. While these correlations are useful for optimizing an existing bioreactor, they are of limited use when designing a bioreactor with a novel geometry. Designing a new bioreactor vessel requires selecting the proper hardware (i.e., impeller or sparger), which negates the assumption of constant geometry and makes the existing correlations useless. The original scope of this study was to reduce the effort and time required to design and optimize our multichamber single-use bioreactor, however, the developed formula can also be extended to optimize and predict the performance of other stirred-tank reactors.

NOTATION

D	diameter of impeller (m)
T	diameter of vessel (m)
d_{sp}	diameter of ring sparger (m)
d_h	diameter of the holes in the sparger (m)
Q	gas flow rate (L/s)
VVM	volume of air per volume of liquid per minute
ρ_i	density of phase *i* (kg/m^3), where *i* = G (gas) or L (liquid) phase
μ_i	molecular viscosity of phase *i* (kg/m/s)
σ_L	water-air interfacial tension (N/m)
k	turbulent kinetic energy (m^2/s^2)
ε	turbulent energy dissipation rate (m^2/s^3)
α_i	volume fraction of phase *i*
$\boldsymbol{U_i}$	velocity vector of phase *i* (m/s)
p	pressure (N/m^2)
$\boldsymbol{\tau_{ef}}$	stress tensor (N/m^2)
$\boldsymbol{R_i}$	interphase momentum exchange term (N/m^3)
$\boldsymbol{F_i}$	centrifugal forces (N/m^3)
g	acceleration due to gravity (m/s^2)
C_D	drag coefficient
Re_P	Reynolds number
$\mu_{t,\,L}$	liquid phase turbulent viscosity (kg/m.s)
C_μ, $C_{1\varepsilon}$, $C_{2\varepsilon}$, σ_k, σ_ε	model parameters given the values 0.09, 1.44, 1.92, 1.0, and 1.3, respectively
G_k	rate of production of turbulent kinetic energy (m^2/s^4)
$\prod_{kL}$, $\prod_{\varepsilon L}$	terms accounting for influence of continuous phase on dispersed phase
n_i	number density of bubbles in the i^{th} bubble class
B_{iB}	birth rate due to breakage (m^{-3}/s)
D_{iB}	death rate due to breakage (m^{-3}/s)
B_{iC}	birth rate due to coalescence (m^{-3}/s)
D_{iC}	death rate due to coalescence (m^{-3}/s)
$a(V, V')$	coalescence rate prevalent between the different sized bubbles of volumes V and V' (s^{-1})
b(V')	breakage rate of bubble with volume V' (s^{-1})
m(V')	number of daughter bubbles formed due to fragmentation from bubbles of volume V'
n(V,t)	number of bubbles of volume V at time t
$p(V, V')$	probability density function to determine offspring bubbles of volume V generated from bubbles of volume V'
f_i	ratio of volume fraction of i^{th} group bubbles and total gas volume fraction
d_{32}	Sauter mean diameter of air bubbles
D_{O_2}	molecular diffusivity of O_2 (m^2/s)
k_La	volume averaged mass transfer coefficient (s^{-1})
a	interfacial area (m^2)
d_P	bubble diameter (m)
P	impeller power input (W)
V	volume of liquid (m^3)
n	stirrer rotational speed (s^{-1})
N_e	impeller power number

ORCID

Joshua D. Ramsey https://orcid.org/0000-0002-5872-5595

REFERENCES

1. Singh V. Disposable bioreactor for cell culture using wave-induced agitation. *Cytotechnology*. 1999;30(1):149-158.
2. Brecht R. Disposable bioreactors: Maturation into pharmaceutical glycoprotein manufacturing. *Disposable bioreactors*. Berlin, Heidelberg: Springer; 2009:1-31.
3. De Wilde D, Dreher T, Zahnow C, et al. Superior scalability of single-use bioreactors. *Innovations in Cell Culture*. 2014;14:14-19.
4. Eibl R, Löffelholz C, Eibl D. Single-Use Bioreactors—An Overview. In: Eibl R, Eibl D, editors. *Single-Use Technology in Biopharmaceutical Manufacture*. New York: John Wiley & Sons, Inc.; 2010:33-51.
5. Noack U, De Wilde D, Verhoeye F, et al. Single-Use Stirred Tank Reactor BIOSTAT CultiBag STR: Characterization and Applications. In: Eibl R, Eibl D, editors. *Single-Use Technology in Biopharmaceutical Manufacture*. New York: John Wiley & Sons, Inc.; 2010:225-240.
6. Morrow K. Disposable bioreactors gaining favor: New components and systems improve process reliability and reduce cost. *Genetic Engineering News*. 2006;12:26-12.
7. Levine HL, Stock R, Lilja JE, et al. Single-use technology and modular construction. *BioProcess Int*. 2013;11:40-45.
8. Amer M, Ramsey JD. Multi-chamber single-use bioreactor–a proof of concept prototype. *Biochem Eng J*. 2018;130:113-120.
9. Chisti Y. Hydrodynamic damage to animal cells. *Crit Rev Biotechnol*. 2001;21(2):67-110.
10. Harvey P, Greaves M. Turbulent flow in an agitated vessel. Part I: A predictive model. *Trans IChemE*. 1982;60:195-200.
11. Harvey P, Greaves M. Turbulent flow in an agitated vessel, part II: Numerical solution and model predictions. *Trans Inst Chem Eng*. 1982;60:201-210.
12. Pericleous KA, Patel M. The modelling of tangential and axial agitators in chemical reactors. *Physicochem hydrodynam*. 1987;8(2):105-123.

13. Placek J, Tavlarides L, Smith G, Fořt I. Turbulent flow in stirred tanks. Part II: A two-scale model of turbulence. *AIChE J*. 1986;32(11):1771-1786.
14. Joshi J, Sahu A, Kumar P. LDA measurements and CFD simulations of flow generated by impellers in mechanically agitated reactors. *Sadhana*. 1998;23(5–6):505-539.
15. Gimbun J, Rielly CD, Nagy ZK. Modelling of mass transfer in gas–liquid stirred tanks agitated by Rushton turbine and CD-6 impeller: A scale-up study. *Chem Eng Res Design*. 2009;87(4):437-451.
16. Laakkonen M, Moilanen P, Alopaeus V, Aittamaa J. Modelling local bubble size distributions in agitated vessels. *Chem Eng Sci*. 2007;62(3):721-740.
17. Laakkonen M, Moilanen P, Alopaeus V, Aittamaa J. Modelling local gas–liquid mass transfer in agitated vessels. *Chem Eng Res Design*. 2007;85(5):665-675.
18. Oshinowo LM, Bakker A. CFD modeling of solids suspensions in stirred tanks. Paper presented at: Symposium on Computational Modelling of Metals, Minerals and Materials, TMS Annual Meeting. Seattle, WA2002.
19. Torré J-P, Fletcher DF, Lasuye T, Xuereb C. Single and multiphase CFD approaches for modelling partially baffled stirred vessels: Comparison of experimental data with numerical predictions. *Chem Eng Sci*. 2007;62(22):6246-6262.
20. Wang F, Mao Z-S, Wang Y, Yang C. Measurement of phase holdups in liquid–liquid–solid three-phase stirred tanks and CFD simulation. *Chem Eng Sci*. 2006;61(22):7535-7550.
21. Qi N, Zhang H, Zhang K, Xu G, Yang Y. CFD simulation of particle suspension in a stirred tank. *Particuology*. 2013;11(3):317-326.
22. Löffelholz C, Kaiser SC, Werner S, Eibl D. CFD as a tool to characterize single-use bioreactors. In: Eibl R, Eibl D, eds. *Single-Use Technology in Biopharmaceutical Manufacture*. New York: John Wiley & Sons, Inc.; 2010:263-279.
23. Kazemzadeh A, Elias C, Tamer M, Ein-Mozaffari F. Hydrodynamic performance of a single-use aerated stirred bioreactor in animal cell culture: Applications of tomography, dynamic gas disengagement (DGD), and CFD. *Bioprocess Biosyst Eng*. 2018;41(5):679-695.
24. Odeleye A, Marsh D, Osborne M, Lye G, Micheletti M. On the fluid dynamics of a laboratory scale single-use stirred bioreactor. *Chem Eng Sci*. 2014;111:299-312.
25. Kaiser S, Jossen V, Schirmaier C, et al. Fluid flow and cell proliferation of mesenchymal adipose-derived stem cells in small-scale, stirred, single-use bioreactors. *Chemie Ingenieur Technik*. 2013;85(1–2):95-102.
26. Schirmaier C, Jossen V, Kaiser SC, et al. Scale-up of adipose tissue-derived mesenchymal stem cell production in stirred single-use bioreactors under low-serum conditions. *Eng Life Sci*. 2014;14(3):292-303.
27. Rathore A, Sharma C, Persad AA. Use of computational fluid dynamics as a tool for establishing process design space for mixing in a bioreactor. *Biotechnol Prog*. 2012;28(2):382-391.
28. Sarkar J, Shekhawat LK, Loomba V, Rathore AS. CFD of mixing of multi-phase flow in a bioreactor using population balance model. *Biotechnol Prog*. 2016;32(3):613-628.
29. Villiger TK, Neunstoecklin B, Karst DJ, et al. Experimental and CFD physical characterization of animal cell bioreactors: From micro-to production scale. *Biochem Eng J*. 2018;131:84-94.
30. Markopoulos J, Christofi C, Katsinaris I. Mass transfer coefficients in mechanically agitated gas-liquid contactors. *Chem Eng Technol*. 2007;30(7):829-834.
31. ANSYS F. Fluent user's manual. Software release 2006;13.
32. Schiller L. A drag coefficient correlation. *Zeit Ver Deutsch Ing*. 1933;77:318-320.
33. Kaiser SC. Characterization and optimization of single-use bioreactors and biopharmaceutical production processes using computational fluid dynamics. PhD Thesis. Fakultat III Prozesswissenschaften der Technischen Universitat Berlin, Germany; 2015.
34. Kaiser SC, Eibl R, Eibl D. Engineering characteristics of a single-use stirred bioreactor at bench-scale: The Mobius CellReady 3L bioreactor as a case study. *Eng Life Sci*. 2011;11(4):359-368.
35. Bakker A, Van den Akker H. A computational model for the gas-liquid flow in stirred reactors. *Chem Eng Res Design*. 1994;72(A4):594-606.
36. Khopkar A, Rammohan A, Ranade V, Dudukovic M. Gas–liquid flow generated by a Rushton turbine in stirred vessel: CARPT/CT measurements and CFD simulations. *Chem Eng Sci*. 2005;60(8–9):2215-2229.
37. Deen NG, Solberg T, Hjertager BH. Flow generated by an aerated Rushton impeller: Two-phase PIV experiments and numerical simulations. *Can J Chem Eng*. 2002;80(4):1-15.
38. Rizk M, Elghobashi S. A two-equation turbulence model for dispersed dilute confined two-phase flows. *Int J Multiphase Flow*. 1989;15(1):119-133.
39. Zhang H, Zhang K, Fan S. CFD simulation coupled with population balance equations for aerated stirred bioreactors. *Eng Life Sci*. 2009;9(6):421-430.
40. Dhanasekharan KM, Sanyal J, Jain A, Haidari A. A generalized approach to model oxygen transfer in bioreactors using population balances and computational fluid dynamics. *Chem Eng Sci*. 2005;60(1):213-218.
41. Venneker BC, Derksen JJ, Van den Akker HE. Population balance modeling of aerated stirred vessels based on CFD. *AIChE J*. 2002;48(4):673-685.
42. ANSYS FLUENT. Population Balance Module Manual. *Software release*. 2011;14.
43. Sanyal J, Marchisio DL, Fox RO, Dhanasekharan K. On the comparison between population balance models for CFD simulation of bubble columns. *Ind Eng Chem Res*. 2005;44(14):5063-5072.
44. Kálal Z, Jahoda M, Fořt I. Modelling of the bubble size distribution in an aerated stirred tank: Theoretical and numerical comparison of different breakup models. *Chem Process Eng*. 2014;35(3):331-348.
45. Chen P, Sanyal J, Duduković M. Numerical simulation of bubble columns flows: Effect of different breakup and coalescence closures. *Chem Eng Sci*. 2005;60(4):1085-1101.
46. Bordel S, Mato R, Villaverde S. Modeling of the evolution with length of bubble size distributions in bubble columns. *Chem Eng Sci*. 2006;61(11):3663-3673.
47. Podila K, Al Taweel A, Koksal M, Troshko A, Gupta Y. CFD simulation of gas–liquid contacting in tubular reactors. *Chem Eng Sci*. 2007;62(24):7151-7162.
48. Prince MJ, Blanch HW. Bubble coalescence and break-up in air-sparged bubble columns. *AIChE J*. 1990;36(10):1485-1499.
49. Luo H, Svendsen HF. Theoretical model for drop and bubble breakup in turbulent dispersions. *AIChE J*. 1996;42(5):1225-1233.
50. Luo H. Coalescence, breakup and liquid circulation in bubble column reactors. Dr. Ing (Doctoral dissertation), Department of Chemical Engineering, the Norwegian Institute of Technology, Trondheim, Norway, 1993.
51. Chesters AK. Modelling of coalescence processes in fluid-liquid dispersions: A review of current understanding. *Chemical engineering research and design*. 1991;69(A4):259-270.
52. MARTÍNEZ-BAZÁN C, Montanes J, Lasheras JC. On the breakup of an air bubble injected into a fully developed turbulent flow. Part 1. Breakup frequency. *J Fluid Mech*. 1999;401:157-182.
53. Alopaeus V, Koskinen J, Keskinen KI, Majander J. Simulation of the population balances for liquid–liquid systems in a nonideal stirred tank. Part 2—Parameter fitting and the use of the multiblock model for dense dispersions. *Chem Eng Sci*. 2002;57(10):1815-1825.
54. Lehr F, Millies M, Mewes D. Bubble-size distributions and flow fields in bubble columns. *AIChE Journal*. 2002;48(11):2426-2443.
55. Higbie, R. The rate of absorption of a pure gas into a still liquid during short periods of exposure. *Trans AIChE*. 1935;31:365-389.

56. Panneerselvam R, Savithri S, Surender GD. CFD modeling of gas-liquid-solid mechanically agitated contactor. *Chemical Engineering Research and Design* 2008;86(12):1331-1344.
57. Kaiser SC, Löffelholz C, Sr W, Eibl D. CFD for characterizing standard and single-use stirred cell culture bioreactors. *Computational fluid dynamics technologies and applications*. London, UK: InTech; 2011.
58. Rewatkar V, Deshpande A, Pandit A, Joshi J. Gas hold-up behavior of mechanically agitated gas-liquid reactors using pitched blade downflow turbines. *Can J Chem Eng*. 1993;71(2):226-237.
59. McFarlane CM, Zhao XM, Nienow AW. Studies of high solidity ratio hydrofoil impellers for aerated bioreactors. 2. Air—Water studies. *Biotechnol Prog*. 1995;11(6):608-618.
60. Birch D, Ahmed N. The influence of sparger design and location on gas dispersion in stirred vessels. *Chemical Engineering Research and Design*. 1997;75(5):487-496.
61. García-Cortés D, Xuereb C, Taillandier P, Jáuregui-Haza U, Bertrand J. Effect of dual impeller-Sparger geometry on the hydrodynamics and mass transfer in stirred vessels. *Chemical Engineering & Technology: Industrial Chemistry-Plant Equipment-Process Engineering-Biotechnology*. 2004; 27(9):988-999.
62. Nienow A. Gas dispersion performance in fermenter operation. *Chem Eng Prog*. 1990;86(2):61-71.

How to cite this article: Amer M, Feng Y, Ramsey JD. Using CFD simulations and statistical analysis to correlate oxygen mass transfer coefficient to both geometrical parameters and operating conditions in a stirred-tank bioreactor. *Biotechnol Progress*. 2019;e2785. https://doi.org/10.1002/btpr.2785